

# Model-based Reconstruction for Simultaneous Multi-slice T1 Mapping using Single-shot Inversion-recovery Radial FLASH

Xiaoqing Wang<sup>1,2\*</sup>, Sebastian Rosenzweig<sup>1,2</sup>, Nick Scholand<sup>1,2</sup>, H.Christian M.Holme<sup>1,2</sup>,  
and Martin Uecker<sup>1,2</sup>

<sup>1</sup>Department of Interventional and Diagnostic Radiology of the University Medical Center Göttingen, 37075, Germany

<sup>2</sup>DZHK (German Centre for Cardiovascular Research), Partner Site Göttingen, Berlin, Germany

July 22, 2022

## Abstract

**Purpose:** To develop a simultaneous multi-slice (SMS) model-based reconstruction method combined with inversion recovery (IR) radial SMS fast low-angle shot (FLASH) sequences for accelerated multi-slice T1 mapping.

**Methods:** This work extends single-slice model-based reconstruction to SMS by modeling the estimation of parameter maps from simultaneously acquired slices and the respective coil sensitivities as a single nonlinear inverse problem. This strategy enables an arbitrary choice of SMS acquisition in the partition dimension. Two IR radial SMS sampling schemes with FLASH readout are investigated. Validations have been performed on SMS phantom, human brain and abdominal studies.

**Results:** Phantom results confirm good T1 accuracy and precision of the proposed SMS model-based reconstructions in comparison to the single-slice IR references. In-vivo human brain studies show a better performance of the SMS rotated golden-angle scheme than the SMS aligned one as well as the conventional multi-slice acquisition using model-based reconstructions. The former could achieve simultaneous 5-slice human brain T1 mapping or 3-slice abdominal T1 mapping within a single inversion recovery of 4 s. A full-brain T1 mapping with a resolution of  $0.75 \times 0.75 \times 5 \text{ mm}^3$  is then feasible within 1 minute.

**Conclusion:** The extension of single-slice model-based reconstruction for SMS data acquisitions was implemented and demonstrated for efficient high-resolution multi-slice T1 mapping.

**Keywords:** model-based reconstruction, simultaneous multi-slice, T1 mapping, radial FLASH

---

\*Xiaoqing Wang PhD, Department of Interventional and Diagnostic Radiology of the University Medical Center Göttingen, 37075, Germany  
xiaoqing.wang@med.uni-goettingen.de

# Introduction

Quantitative T1 mapping finds increasing applications in a variety of clinical usage [1, 2]. Fast T1 mapping usually employs the inversion recovery (IR) Look-Locker (LL) sequence where RF excitations are continuously applied after inversion followed by T1 determination in a postprocessing step [3–5]. While the conventional IR LL method requires segmented data acquisitions with multiple inversions [4, 5], recent advances in non-Cartesian sampling [6–10], compressed sensing [10–12] as well as real-time MRI [9, 13] have enabled single-slice T1 mapping within a single inversion recovery. On the other hand, parameter maps can be estimated directly from undersampled k-space using model-based reconstructions [7, 14–21]. In this way, only the parameter maps instead of a number of contrast-weighted images have to be reconstructed, making this kind of method an interesting alternative for quantitative MRI. Such strategies have enabled single-shot high-resolution T1 mapping with high accuracy and precision as well [18, 20, 22].

So far, most of the above efforts have focused on the acceleration of single-slice parameter mapping. However, in clinical diagnosis, multi-slice parameter mapping is highly desirable [23–25]. Methods exploiting the conventional multi-slice acquisition strategy have been reported [23, 24, 26, 27]. On the other hand, simultaneous multi-slice (SMS) technique [28] is a promising way to accelerate multi-slice quantitative MRI. SMS allows distributing undersampling along the additional slice dimension and exploits sensitivity encoding in all three spatial dimensions. Applications of SMS in quantitative MRI include but are not limited to simultaneous 3-slice MR fingerprinting [29], 3-slice cardiac T1 mapping based on the SAPPHIRE technique [25] and 3 to 5-slice T2 mapping using the Cartesian multi-echo spin-echo method [30].

In this work, we aim to combine both the advantages of model-based reconstructions and radial SMS acquisition strategies with FLASH readout for accelerated multi-slice T1 mapping. In particular, we develop a general calibrationless SMS model-based reconstruction framework that formulates the estimation of parameter maps and coil sensitivities from all slices as a single inverse problem. This strategy enables arbitrary sampling schemes for SMS acquisitions. Following our previous work on radial SMS parallel imaging using nonlinear inversion (NLINV) [31], this work investigates two IR radial SMS acquisition schemes using the developed model-based reconstructions. Performance of the proposed method is validated on the phantom, human brain and abdominal studies.

## Theory

### SMS Acquisition

In this study, we use similar radial SMS sampling strategies for IR LL SMS data acquisition as in [31]. I.e., following a non-selective inversion, SMS data is sampled continuously using a tiny golden angle ( $\approx 23.63^\circ$ ) [32], with radial spokes distributed either with aligned or rotated angles along the partition dimension. The additional Figure 1 demonstrates these two sampling methods together with a conventional multi-slice acquisition scheme. The SMS aligned scenario allows the decoupling of partitions using an inverse Fourier transform, enabling independent reconstruction of all slices. In such a way, there is still an SNR benefit of SMS over the conventional multi-slice scheme. However, the main advantage of SMS - acceleration in the direction perpendicular to the slices - only comes into play when distinct k-space samples are acquired [31, 33]. Additional Figure 1 (bottom left) presents the latter sampling scheme, where a better k-space coverage is achieved, especially with a golden-angle method [31]. To reconstruct images/parameter maps with the SMS golden-angle acquisition, the conventional slice-by-slice reconstruction no longer applies, a more general SMS model-based reconstruction method is therefore developed, which is explained in the

following.

## SMS Model-based Reconstruction

Following a similar notation introduced in [31], we define  $p, q \in \{1, \dots, Q\}$  the partition index and the slice index, respectively, with  $Q$  the total number of partitions/slices. In SMS acquisitions, signal from the  $p$ th partition  $\tilde{\mathbf{y}}^p$  can be written as:

$$\tilde{\mathbf{y}}^p = \sum_{q=1}^Q \xi^{p,q} \mathbf{y}^q \quad (1)$$

with  $\xi^{p,q}$  being an SMS encoding matrix, which is a Fourier matrix in this study, i.e.,  $\xi^{p,q} = \exp\left(-2\pi i \frac{(p-1)(q-1)}{Q}\right)$ . The signal  $\mathbf{y}_j^q(t)$  for the  $q$ th slice of the  $j$ th coil is given by

$$\mathbf{y}_j^q(t) = \int M^q(\vec{r}) c_j^q(\vec{r}) e^{-i\vec{r} \cdot \vec{k}(t)} d\vec{r} \quad (2)$$

where  $c_j^q$  is the corresponding coil sensitivity map,  $\vec{r}$  is the position in image space,  $\vec{k}(t)$  is the chosen k-space trajectory.  $M^q$  is the  $T_1$  relaxation model for the  $q$ th slice:

$$M_{t_k}^q = M_{ss}^q - (M_{ss}^q + M_0^q) \cdot e^{-t_k \cdot R_1^{*q}} \quad (3)$$

with  $t_k$  the time after inversion which is defined as the center of each acquisition window.  $M_{ss}^q$ ,  $M_0^q$  and  $R_1^{*q}$  are the steady-state signal, equilibrium signal and effective relaxation rate, respectively. After estimation of  $(M_{ss}^q, M_0^q, R_1^{*q})$ ,  $T_1$  values of the  $q$ th slice can be calculated by [3, 4]:  $T_1^q = \frac{M_0^q}{M_{ss}^q \cdot R_1^{*q}}$ . To estimate parameter maps and coil sensitivity maps from all the slices, equations (1) and (2) are then understood as a nonlinear inverse problem with a nonlinear operator,  $F$ , mapping all the unknowns from all slices to the measured undersampled SMS data  $\tilde{Y} = (\tilde{\mathbf{y}}_{t_1}^1, \dots, \tilde{\mathbf{y}}_{t_1}^Q, \tilde{\mathbf{y}}_{t_2}^1, \dots, \tilde{\mathbf{y}}_{t_n}^Q)^T$ :

$$F : x \mapsto P\Xi \begin{pmatrix} \mathcal{F}\{\mathbf{c}^1 \cdot \mathbf{M}_{t_1}^1\} \\ \vdots \\ \mathcal{F}\{\mathbf{c}^Q \cdot \mathbf{M}_{t_1}^Q\} \\ \mathcal{F}\{\mathbf{c}^1 \cdot \mathbf{M}_{t_2}^1\} \\ \vdots \\ \mathcal{F}\{\mathbf{c}^Q \cdot \mathbf{M}_{t_n}^Q\} \end{pmatrix}, \quad \text{with } P\Xi := \begin{pmatrix} P_{t_1}\xi & & & 0 \\ & P_{t_2}\xi & & \\ & & \ddots & \\ 0 & & & P_{t_n}\xi \end{pmatrix} \quad (4)$$

$$\text{and } \mathcal{F}\{\mathbf{c}^q \cdot \mathbf{M}_{t_k}^q\} := \begin{pmatrix} \mathcal{F}\{c_1^q \cdot M_{t_k}^q(M_{ss}, M_0, R_1^*)\} \\ \vdots \\ \mathcal{F}\{c_N^q \cdot M_{t_k}^q(M_{ss}, M_0, R_1^*)\} \end{pmatrix}. \quad (5)$$

Here  $P$  is the orthogonal projection onto the trajectory,  $\mathcal{F}$  is the two dimensional Fourier transform.  $\mathbf{c}^q$  represents a set of coil sensitivity maps for the  $q$ th slice.  $M_{t_k}^q(\cdot)$  is the relaxation model prescribed in equation (3). The unknowns are  $x = (x^1, \dots, x^q, \dots, x^Q)^T$  with  $x^q = (M_{ss}^q, M_0^q, R_1^{*q}, c_1^q, \dots, c_N^q)^T$ , which are then estimated by solving the following regularized nonlinear inverse problem:

$$\hat{x} = \arg \min_{x \in D} \|F(x) - \tilde{Y}\|_2^2 + \alpha \sum_{q=1}^Q R(x_{\mathbf{p}}^q) + \beta \sum_{q=1}^Q U(x_{\mathbf{c}}^q) \quad (6)$$

with  $R(\cdot)$  the joint  $\ell_1$ -Wavelet regularization in the parameter dimension [20],  $U(\cdot)$  the Sobolev norm [34] enforcing the smoothness of coil sensitivity maps.  $x_{\mathbf{p}}^q = (M_{ss}^q, M_0^q, R_1^{*q})^T$  and  $x_{\mathbf{c}}^q = (c_1^q, \dots, c_N^q)^T$ ,  $\alpha$  and  $\beta$  are the regularization parameters for parameter maps and coil sensitivity maps, respectively.  $D$  is a convex set ensuring  $R_1^{*q}$  to be nonnegative. The above nonlinear inverse problem is then solved by the iteratively regularized Gauss-Newton method (IRGNM) where in each Gauss-Newton step the nonlinear problem was linearized and solved by the fast iterative shrinkage-thresholding algorithm (FISTA) [35]. More details of the IRGNM-FISTA algorithm can be found in [20].

## Methods

### Data Acquisition

All MRI experiments were conducted on a Magnetom Skyra 3T (Siemens Healthineers, Erlangen, Germany) with approval of the local ethics committee. The proposed method was first validated on a commercial reference phantom (Diagnostic Sonar LTD, Scotland, UK) consisting of six compartments with defined T1 values surrounded by water. Phantom and brain studies were conducted with a 20-channel head/neck coil, whereas abdominal scans were performed with a combined thorax and spine coil with 26 channels. During technical developments, 3 volunteers without known illness were recruited. In all experiments, simultaneously acquired slices using IR radial FLASH are separated by a fixed distance  $d$ . All single-slice and multi-slice acquisitions employed the same nominal flip angle  $\alpha = 6^\circ$ . Acquisition parameters for phantom and brain measurements were: FOV:  $192 \times 192 \text{ mm}^2$ , matrix size:  $256 \times 256$ , TR/TE = 4.10/2.58 ms, bandwidth 630 Hz/pixel, slice thickness  $\Delta z = 5 \text{ mm}$ , slice distances  $d = 15 \text{ mm}$  and  $d = 20 \text{ mm}$  for phantom and brain studies, respectively. A gold standard T1 mapping was performed on the center slice of the phantom using an IR spin-echo method [36] with 9 IR scans (TI=30, 530, 1030, 1530, 2030, 2530, 3030, 3530, 4030 ms), TR/TE = 4050/12 ms, FOV:  $192 \times 192 \text{ mm}^2$ , matrix size:  $192 \times 192$ , and a total acquisition time of 2.4 hours. Parameters for the abdominal measurements were: FOV:  $256 \times 256 \text{ mm}^2$ , matrix size:  $192 \times 192$ , TR/TE = 3.10/1.88 ms, bandwidth 850 Hz/pixel,  $\Delta z = 6 \text{ mm}$ ,  $d = 20 \text{ mm}$ . All single-shot measurements were acquired within 4 seconds. Abdominal experiments were performed during a brief breathhold.

### Image Reconstruction

Image reconstruction was done offline based on the C-based software package BART [37] on a 40-core 2.3 GHz Intel Xeon E5-2650 PC with a RAM size of 500 GB. Followed by the gradient delay corrections [38] and channel compression to 8 principle components, the multi-coil radial raw data were gridded onto a Cartesian grid, where all successive iterations were performed [39]. Similar to the single-slice case [20], parameter maps  $(M_{ss}^q, M_0^q, R_1^{*q})^T$  were initialized with  $(1.0, 1.0, 1.5)^T$  and all coil sensitivities zeros for all slices. 10 Gauss-Newton steps were employed to ensure convergence. The regularization parameters  $\alpha$  and  $\beta$  were initialized with 1 and subsequently reduced by a factor of 3 in each Gauss-Newton step. A minimum value of  $\alpha$  was used to control the noise of the estimated parameter maps at higher Gauss-Newton steps. The optimal value  $\alpha_{\min}$  was chosen by visual observation to optimize SNR without compromising the quantitative accuracy or delineation of structural details. In this study, all multi-slice reconstructions used the same minimum regularization parameter  $\alpha_{\min} = 0.00125$  for fair comparisons.

Model-based reconstruction techniques generally offer a flexible choice of temporal resolution, i.e., even a single radial spoke per k-space frame could be employed for accurate parameter estimation [18]. However, a certain amount of temporal binning may effectively reduce the computational demand as long as the T1

accuracy is not compromised [4, 18]. Here, the number of binned spokes was chosen such that the temporal bin size does not exceed 85 ms. More specifically, 20, 6 and 4 spokes per k-space frame were selected for single-slice, simultaneous 3-slice and 5-slice model-based brain reconstructions, respectively. For abdominal studies, 25 and 8 spokes per k-space frame were used for single-slice and simultaneous 3-slice reconstructions. In the spirit of reproducible research, code and data to reproduce the experiments will be made available on <https://github.com/mrirecon/sms-t1-mapping>.

## Data Analysis

All quantitative T1 results are reported as mean  $\pm$  standard deviation (SD). Regions-of-interest (ROIs) were carefully selected to minimize partial volume errors using arrayShow [40] tool in MATLAB (MathWorks, Natick, MA). For evaluations, the relative difference map ( $\frac{|T1_{estimate} - T1_{ref}|}{|T1_{ref}|} \times 100\%$ ) and the normalized quantitative relative errors ( $\|T1_{estimate} - T1_{ref}\|_2 / \|T1_{ref}\|_2$ ) were calculated, respectively, with  $T1_{ref}$  the reference T1 map estimated from single-slice acquisition [20] and  $T1_{estimate}$  the T1 map reconstructed from the corresponding multi-slice acquisition.

## Results

The proposed SMS model-based reconstruction was first validated on the experimental phantom study with the SMS rotated golden-angle acquisition. Figure 1 shows T1 maps of three slices reconstructed with the proposed method together with an IR spin-echo reference and that estimated from single-slice IR radial acquisition [20] of the center slice. Visual inspection reveals that the proposed method can completely disentangle superposed slices and all quantitative multi-slice T1 maps are in good agreement with the references. These findings are confirmed in the ROI-analyzed T1 values of the center slice in Figure 1 (b), where preservation of good precision (low standard deviation) of the SMS T1 mapping method is also observed. Quantitative results for T1 maps from the other two slices are presented in the additional Table 1, which confirms good T1 accuracy and precision of these two slices as well.

Figure 2 (a) compares model-based reconstructed center-slice T1 maps of a human brain at a multi-slice factor of 3 for all multi-slice schemes. Both SMS methods produce T1 maps with less noise and therefore better SNR than the conventional multi-slice method. Further, the SMS T1 values are closer to the single-slice reference, which is demonstrated by the relative difference maps as well as the quantitative errors. Figure 2(b) shows the comparison of human brain T1 maps at a multi-slice factor of 5. In line with the 3-slice results, both SMS T1 maps have better SNRs and are closer to the reference than the conventional multi-slice method. In this case, the SMS golden-angle method further helps to reduce streaking artifacts that are visible in the border areas of the other two multi-slice T1 maps (indicated by white arrows). Moreover, the SMS golden-angle method has less quantitative errors than the other two multi-slice methods. The ROI-analyzed white- and gray-matter T1 values in Figure 3 confirm the above observations: Apart from similar mean T1 values among all multi-slice methods, both SMS approaches produce T1 values with higher precision (lower standard deviation) than the conventional multi-slice method. Noteworthy, all quantitative brain T1 values are in close agreement with the single-slice reference as well as literature values [41, 42].

Figure 4(a) depicts the T1 maps of a 5-slice SMS golden-angle acquisition as well as the corresponding single-slice T1 maps. All 5-slice T1 maps are visually in good agreement with the corresponding single-slice ones, indicating the combination of SMS rotated golden-angle acquisition and model-based reconstruction could achieve simultaneous 5-slice brain T1 maps within 4 s (i.e., an acceleration factor of 5 compared to

the single-slice case). A similar comparison is presented in the application of simultaneous 3-slice human abdominal T1 mapping in Figure 3(b). Again, good agreement is reached between the simultaneous 3-slice abdominal T1 maps and the single-slice ones (quantitative center-slice liver T1 values: SMS vs single-slice:  $828 \pm 19$  ms vs  $830 \pm 20$  ms), suggesting an acceleration factor of 3 could be achieved for abdominal T1 mapping using the proposed method.

With the above settings, Figure 5 presents a whole-brain T1 mapping of 25 contiguous slices with a resolution of  $0.75 \times 0.75 \times 5$  mm<sup>3</sup>. These 25 T1 maps were acquired using 5 consecutive SMS-5 acquisitions with a slice distance of 25 mm. Each SMS acquisition took 4 seconds with a waiting period of 10 seconds in between to ensure full recovery of the magnetization. Thus, the whole acquisition took 1 minute.

## Discussion

This work describes a SMS model-based reconstruction method combined with IR radial SMS FLASH sequences for efficient multi-slice T1 mapping. The present reconstruction framework models the aliasing of simultaneously acquired slices and their respective coil sensitivities within the data consistency term, formulating the parameter and coil estimation of multiple slices as a single inverse problem. Such a strategy allows for a flexible choice of sampling patterns in SMS acquisitions. Validation results show that the use of SMS model-based reconstruction with the SMS rotated golden-angle scheme could achieve high resolution simultaneous 5-slice brain T1 maps or simultaneous 3-slice abdominal T1 maps within only a single inversion recovery of 4 s. With this technique, a whole-brain T1 mapping is feasible within 1 minute.

For radial sampling, the use of rotated golden-angle in the partition dimension has been proven to have better performance than the aligned scheme for undersampled stack-of-stars 3D volume MRI [33] and 2D radial SMS parallel imaging using NLINV [31]. In this work, we have adopted the same strategy for SMS model-based quantitative parameter mapping. Our results confirm a slightly better performance of this strategy over the aligned scheme, especially at higher acceleration factors. The combination of such a sampling strategy and model-based reconstruction may also be exploited for single-shot SMS myocardial T1 mapping, where part of the IR data (e.g., systolic data) is discarded prior to model-based T1 estimation [43].

In contrast to the aforementioned SMS approaches, the proposed k-space method using model-based reconstructions does not need to compromise between high accuracy using small bin sizes and good quality of intermediately reconstructed images. Furthermore, integration of coil sensitivity estimation into the model-based reconstruction framework helps to avoid pre-calibration scans that are necessary for some other SMS quantitative MRI techniques and this may further reduce any miscalibration errors for parameter mapping.

An alternative to multi-slice T1 mapping is 3D imaging such as the use of a radial stack-of-stars sequence has better SNR benefits than the 2D SMS imaging and could provide 3D isotropic T1 mapping [21]. The proposed model-based reconstruction method is also applicable to 3D T1 mapping. However, 3D sequences need to employ multi-shot/segmented acquisitions, in which case, data over the duration of a complete scan (usually in the order of minutes) have to be combined together for parameter estimation. This makes 3D imaging more sensitive to motion than the 2D SMS counterparts [29]. For example, it would be more challenging for multi-slice abdominal T1 mapping using 3D sequences.

The main limitation of the proposed method is the long computation time, especially for model-based reconstruction of SMS datasets acquired using the rotated golden-angle sampling trajectory: All the data from multiple slices have to be hold in memory simultaneously during iterations, which prevents the entire

computation running on our GPUs. Currently, it took around 10 hours to reconstruct a high-resolution SMS-5 brain dataset using the CPUs. Acceleration of the linearized subproblem such as ideas used in T2 shuffling [44] or double-buffering strategies as proposed in [45] will be employed in the future to reduce reconstruction time.

## Conclusion

The present work extends calibrationless model-based reconstruction to multi-slice T1 mapping with flexible SMS sampling, improving SNR and image quality for high accelerations by exploiting three-dimensional sensitivity encoding.

## Conflict of interest

The authors declare no competing interests.

## References

- [1] Cheng HL, Stikov N, Glugre NR, Wright GA. Practical medical applications of quantitative MR relaxometry. *J. Magn. Reson. Imaging* 2012; 36:805–824.
- [2] Kellman P, Hansen MS. T1-mapping in the heart: accuracy and precision. *J. Cardiovasc. Magn. Reson.* 2014; 16:2.
- [3] Look DC, Locker DR. Time saving in measurement of NMR and EPR relaxation times. *Rev. Sci. Instrum.* 1970; 41:250–251.
- [4] Deichmann R, Haase A. Quantification of T1 values by SNAPSHOT-FLASH NMR imaging. *Journal of Magnetic Resonance (1969)* 1992; 96:608–612.
- [5] Messroghli DR, Radjenovic A, Kozerke S, Higgins DM, Sivananthan MU, Ridgway JP. Modified Look-Locker Inversion recovery (MOLLI) for high-resolution T1 mapping of the heart. *Magn. Reson. Med.* 2004; 52:141–146.
- [6] Winkelmann S, Schaeffter T, Koehler T, Eggers H, Doessel O. An optimal radial profile order based on the Golden Ratio for time-resolved MRI. *IEEE Trans. Med. Imag.* 2007; 26:68–76.
- [7] Tran-Gia J, Stäb D, Wech T, Hahn D, Köstler H. Model-based Acceleration of Parameter mapping (MAP) for saturation prepared radially acquired data. *Magn. Reson. Med.* 2013; 70:1524–1534.
- [8] Gensler D, Mörchel P, Fidler F, Ritter O, Quick HH, Ladd ME, Bauer WR, Ertl G, Jakob PM, Nordbeck P. Myocardial T1: quantification by using an ECG-triggered radial single-shot inversion-recovery MR imaging sequence. *Radiology* 2014; 274:879–887.
- [9] Wang X, Joseph AA, Kalentev O, Merboldt KD, Voit D, Roeloffs VB, van Zalk M, Frahm J. High-resolution myocardial T1 mapping using single-shot inversion recovery fast low-angle shot MRI with radial undersampling and iterative reconstruction. *The British journal of radiology* 2016; 89:20160255.

- [10] Marty B, Coppa B, Carlier P. Fast, precise, and accurate myocardial T1 mapping using a radial MOLLI sequence with FLASH readout. *Magn. Reson. Med.* 2018; 79:1387–1398.
- [11] Doneva M, Börnert P, Eggers H, Stehning C, S n gas J, Mertins A. Compressed sensing reconstruction for magnetic resonance parameter mapping. *Magn. Reson. Med.* 2010; 64:1114–1120.
- [12] Feng L, Benkert T, Block KT, Sodickson DK, Otazo R, Chandarana H. Compressed sensing for body MRI. *J. Magn. Reson. Imaging* 2017; 45:966–987.
- [13] Uecker M, Zhang S, Voit D, Karaus A, Merboldt KD, Frahm J. Real-time MRI at a resolution of 20 ms. *NMR Biomed.* 2010; 23:986–994.
- [14] Block KT, Uecker M, Frahm J. Model-Based Iterative Reconstruction for Radial Fast Spin-Echo MRI. *IEEE Trans. Med. Imaging* 2009; 28:1759–1769.
- [15] Sumpf TJ, Uecker M, Boretius S, Frahm J. Model-based nonlinear inverse reconstruction for T2 mapping using highly undersampled spin-echo MRI. *J. Magn. Reson. Imaging* 2011; 34:420–428.
- [16] Zhao B, Lam F, Liang ZP. Model-based MR parameter mapping with sparsity constraints: parameter estimation and performance bounds. *IEEE Trans. Med. Imaging* 2014; 33:1832–1844.
- [17] Peng X, Liu X, Zheng H, Liang D. Exploiting parameter sparsity in model-based reconstruction to accelerate proton density and T2 mapping. *Medical engineering & physics* 2014; 36:1428–1435.
- [18] Roeloffs V, Wang X, Sumpf TJ, Untenberger M, Voit D, Frahm J. Model-based reconstruction for T1 mapping using single-shot inversion-recovery radial FLASH. *Int. J. Imag. Syst. Tech.* 2016; 26:254–263.
- [19] Zhao B, Setsompop K, Ye H, Cauley SF, Wald LL. Maximum likelihood reconstruction for magnetic resonance fingerprinting. *IEEE Trans. Med. Imaging* 2016; 35:1812–1823.
- [20] Wang X, Roeloffs V, Klosowski J, Tan Z, Voit D, Uecker M, Frahm J. Model-based T1 mapping with sparsity constraints using single-shot inversion-recovery radial FLASH. *Magn. Reson. Med.* 2018; 79:730–740.
- [21] Maier O, Schoormans J, Schloegl M, Strijkers GJ, Lesch A, Benkert T, Block T, Coolen BF, Bredies K, Stollberger R. Rapid T1 quantification from high resolution 3D data with model-based reconstruction. *Magn. Reson. Med.* 2019; 81:2072–2089.
- [22] Tran-Gia J, Wech T, Bley T, K stler H. Model-based acceleration of Look-Locker T1 mapping. *PLoS one* 2015; 10:e0122611.
- [23] Shah NJ, Zaitsev M, Steinhoff S, Zilles K. A new method for fast multislice T1 mapping. *Neuroimage* 2001; 14:1175–1185.
- [24] Deichmann R. Fast high-resolution T1 mapping of the human brain. *Magn. Reson. Med.* 2005; 54:20–27.
- [25] Weing rtner S, Moeller S, Schmitter S, Auerbach E, Kellman P, Shenoy C, Ak akaya M. Simultaneous multislice imaging for native myocardial T1 mapping: Improved spatial coverage in a single breath-hold. *Magn. Reson. Med.* 2017; 78:462–471.
- [26] Wang X, Voit D, Roeloffs V, Uecker M, Frahm J. Fast interleaved multislice T1 mapping: Model-based reconstruction of single-shot inversion-recovery radial FLASH. *Comput. Math. Methods Med.*, 2018; 2018:2560964.
- [27] Li Z, Bilgin A, Johnson K, Galons JP, Vedantham S, Martin DR, Altbach MI. Rapid high-resolution T1 mapping using a highly accelerated radial steady-state free-precession technique. *J. Magn. Reson. Imaging* 2019; 49:239–252.



- [28] Barth M, Breuer F, Koopmans PJ, Norris DG, Poser BA. Simultaneous multislice (SMS) imaging techniques. *Magn. Reson. Med.* 2016; 75:63–81.
- [29] Ye H, Cauley SF, Gagoski B, Bilgic B, Ma D, Jiang Y, Du YP, Griswold MA, Wald LL, Setsompop K. Simultaneous multislice magnetic resonance fingerprinting (SMS-MRF) with direct-spiral slice-GRAPPA (ds-SG) reconstruction. *Magn. Reson. Med.* 2017; 77:1966–1974.
- [30] Hilbert T, Schulz J, Marques JP, Thiran JP, Krueger G, Norris DG, Kober T. Fast model-based T2 mapping using SAR-reduced simultaneous multislice excitation. *Magn. Reson. Med.* 2019; 82:2090–2103.
- [31] Rosenzweig S, Holme HCM, Wilke RN, Voit D, Frahm J, Uecker M. Simultaneous multi-slice MRI using cartesian and radial FLASH and regularized nonlinear inversion: SMS-NLINV. *Magn. Reson. Med.* 2018; 79:2057–2066.
- [32] Wundrak S, Paul J, Ulrici J, Hell E, Geibel MA, Bernhardt P, Rottbauer W, Rasche V. Golden ratio sparse MRI using tiny golden angles. *Magn. Reson. Med.* 2016; 75:2372–2378.
- [33] Zhou Z, Han F, Yan L, Wang DJ, Hu P. Golden-ratio rotated stack-of-stars acquisition for improved volumetric MRI. *Magn. Reson. Med.* 2017; 78:2290–2298.
- [34] Uecker M, Hohage T, Block KT, Frahm J. Image reconstruction by regularized nonlinear inversion - joint estimation of coil sensitivities and image content. *Magn. Reson. Med.* 2008; 60:674–682.
- [35] Beck A, Teboulle M. Fast gradient-based algorithms for constrained total variation image denoising and deblurring problems. *IEEE Trans. Image Processing* 2009; 18:2419–2434.
- [36] Barral JK, Gudmundson E, Stikov N, Etezadi-Amoli M, Stoica P, Nishimura DG. A robust methodology for in vivo T1 mapping. *Magn. Reson. Med.* 2010; 64:1057–1067.
- [37] Uecker M, Ong F, Tamir JI, Bahri D, Virtue P, Cheng JY, Zhang T, Lustig M. Berkeley advanced reconstruction toolbox. In: *Proc. Intl. Soc. Mag. Reson. Med.* 23, Toronto, 2015. p. 2486.
- [38] Block KT, Uecker M. Simple method for adaptive gradient-delay compensation in radial MRI. In: *Proc. Intl. Soc. Mag. Reson. Med.* 19, Montreal, 2011. p. 2816.
- [39] Wajer FTAW, Pruessmann KP. Major speedup of reconstruction for sensitivity encoding with arbitrary trajectories. In: *Proc. Intl. Soc. Mag. Reson. Med.* 9, Glasgow, 2001. p. 0767.
- [40] Sumpf T, Unterberger M. arrayShow: a guide to an open source matlab tool for complex MRI data analysis. In: *Proc. Intl. Soc. Mag. Reson. Med.* 21, Salt Lake City, 2013. p. 2719.
- [41] Wansapura JP, Holland SK, Dunn RS, Ball Jr WS. NMR relaxation times in the human brain at 3.0 tesla. *J. Magn. Reson. Imaging* 1999; 9:531–538.
- [42] Preibisch C, Deichmann R. Influence of RF spoiling on the stability and accuracy of T1 mapping based on spoiled FLASH with varying flip angles. *Magn. Reson. Med.* 2009; 61:125–135.
- [43] Wang X, Kohler F, UnterbergBuchwald C, Lotz J, Frahm J, Uecker M. Model-based myocardial T1 mapping with sparsity constraints using single-shot inversion-recovery radial FLASH cardiovascular magnetic resonance. *J. Cardiovasc. Magn. Reson.* 2019; 21:60.
- [44] Tamir JI, Uecker M, Chen W, Lai P, Alley MT, Vasanawala SS, Lustig M. T2 shuffling: Sharp, multicontrast, volumetric fast spin-echo imaging. *Magn. Reson. Med.* 2017; 77:180–195.
- [45] Maier O, Schloegl M, Bredies K, Stollberger R. 3D model-based parameter quantification on resource constrained hardware using double-buffering. In: *Proc. Intl. Soc. Mag. Reson. Med.* 27, Montreal, 2019. p. 4839.

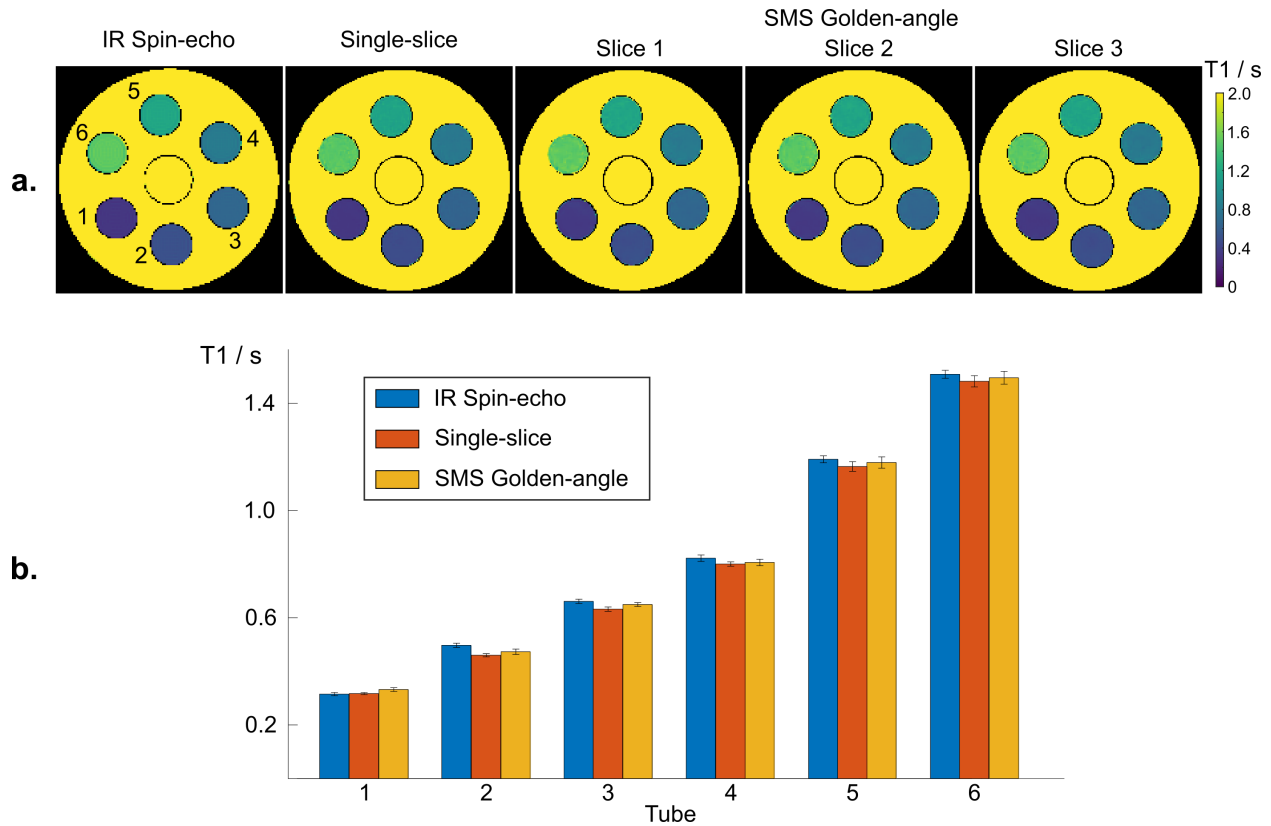


Figure 1: **a.** T1 maps from an experimental phantom acquired with a 3-slice SMS rotated golden-angle IR FLASH and reconstructed using the model-based algorithm. For the center slice, an IR spin-echo T1 map with conventional reconstruction and a T1 map from a single-slice IR FLASH acquisition with model-based reconstruction are presented as reference. **b.** Quantitative T1 values (mean and standard deviation) within ROIs of the six phantom tubes for the center-slice T1 maps of all three methods.

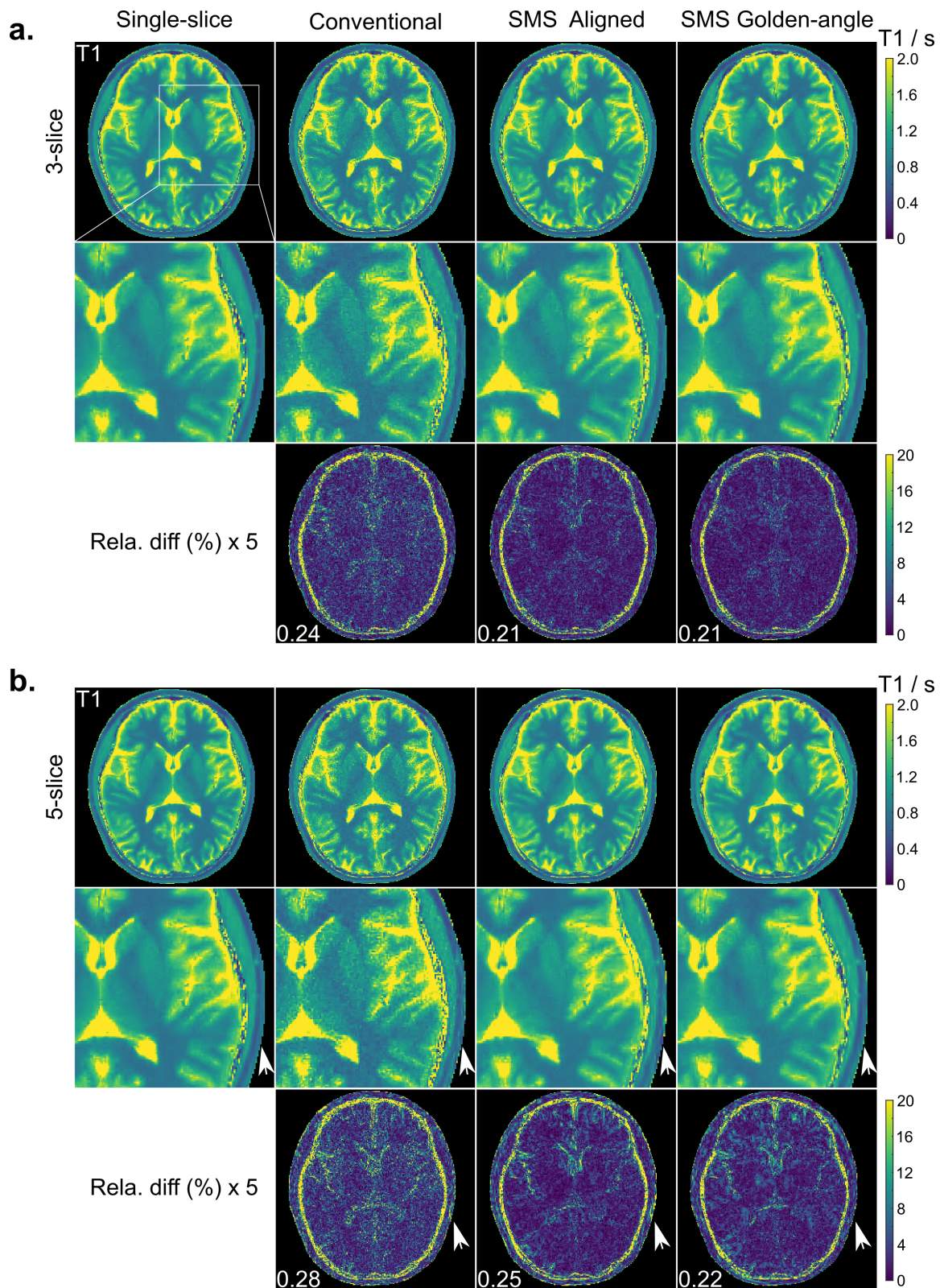


Figure 2: **a.** (Top) Center slice of three brain T1 maps from different multi-slice acquisitions using model-based reconstruction with (middle) magnified T1 regions and (bottom) their relative difference maps ( $\times 5$ ) to the single-slice reference T1 map. **b.** Similar comparisons at a multi-slice factor of 5. Normalized quantitative errors are presented at the bottom left of all relative-difference T1 maps. Note that streakings in the border areas are better removed (white arrows) using SMS rotated golden-angle acquisition with model-based reconstruction.

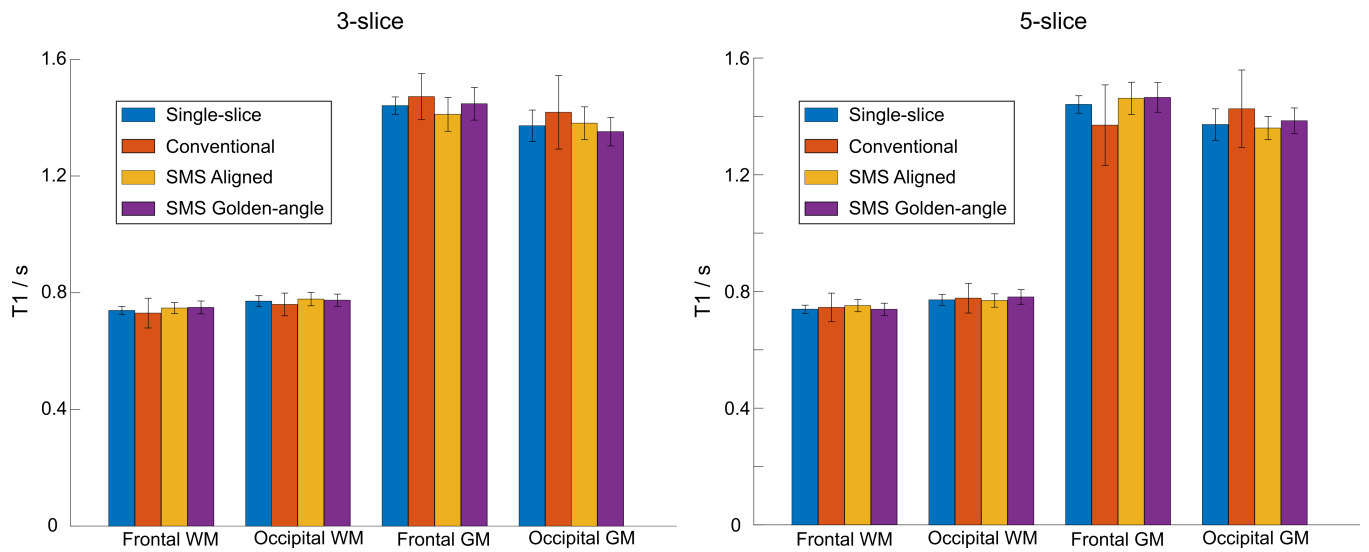


Figure 3: Quantitative T1 values (mean and standard deviation) within ROIs that were manually drawn into the frontal white matter (WM), occipital WM, frontal gray matter (GM) and occipital GM of all T1 maps in Figure 2.

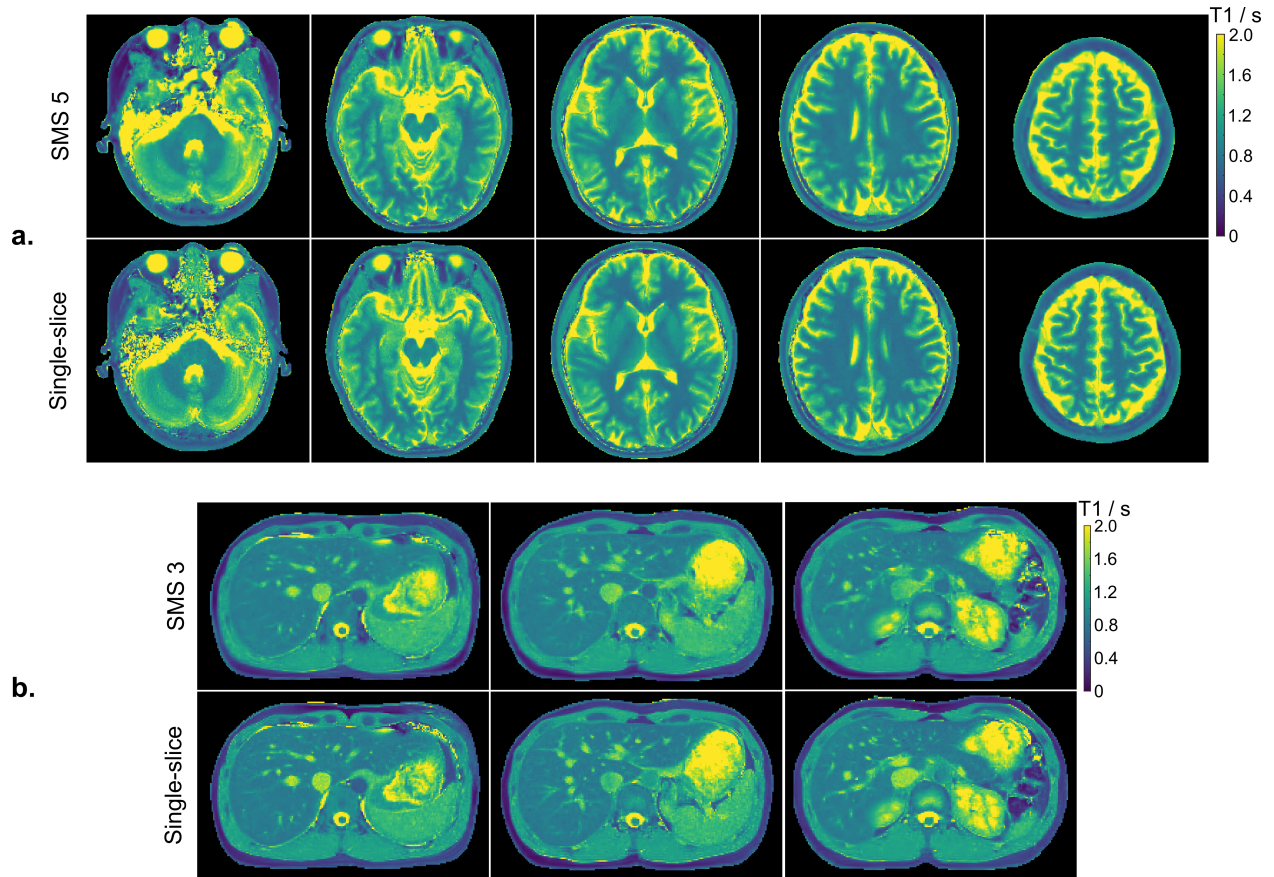


Figure 4: **a.** (Top) Simultaneous 5-slice brain T1 maps estimated using SMS rotated golden-angle acquisition and model-based reconstructions. (Bottom) The corresponding single-slice T1 maps. **b.** Similar comparisons for simultaneous 3-slice abdominal T1 mapping. The abdominal acquisition was performed within a single breathhold of 4 s.

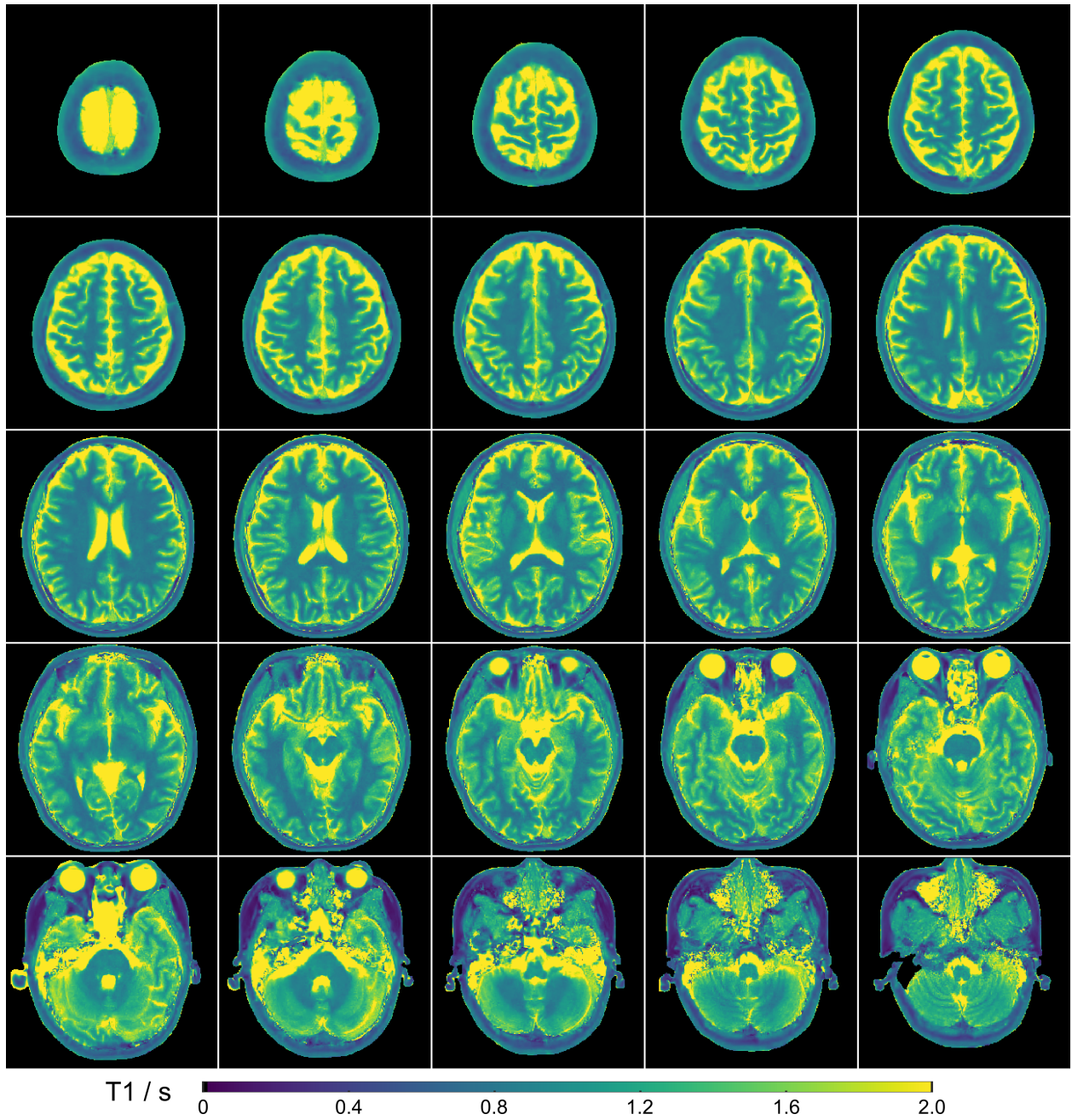


Figure 5: Full brain T1 maps of 25 contiguous slices at a resolution of  $0.75 \times 0.75 \times 5 \text{ mm}^3$ . These 25 T1 maps were acquired using 5 consecutive 5-slice SMS acquisitions with a slice distance of 25 mm.

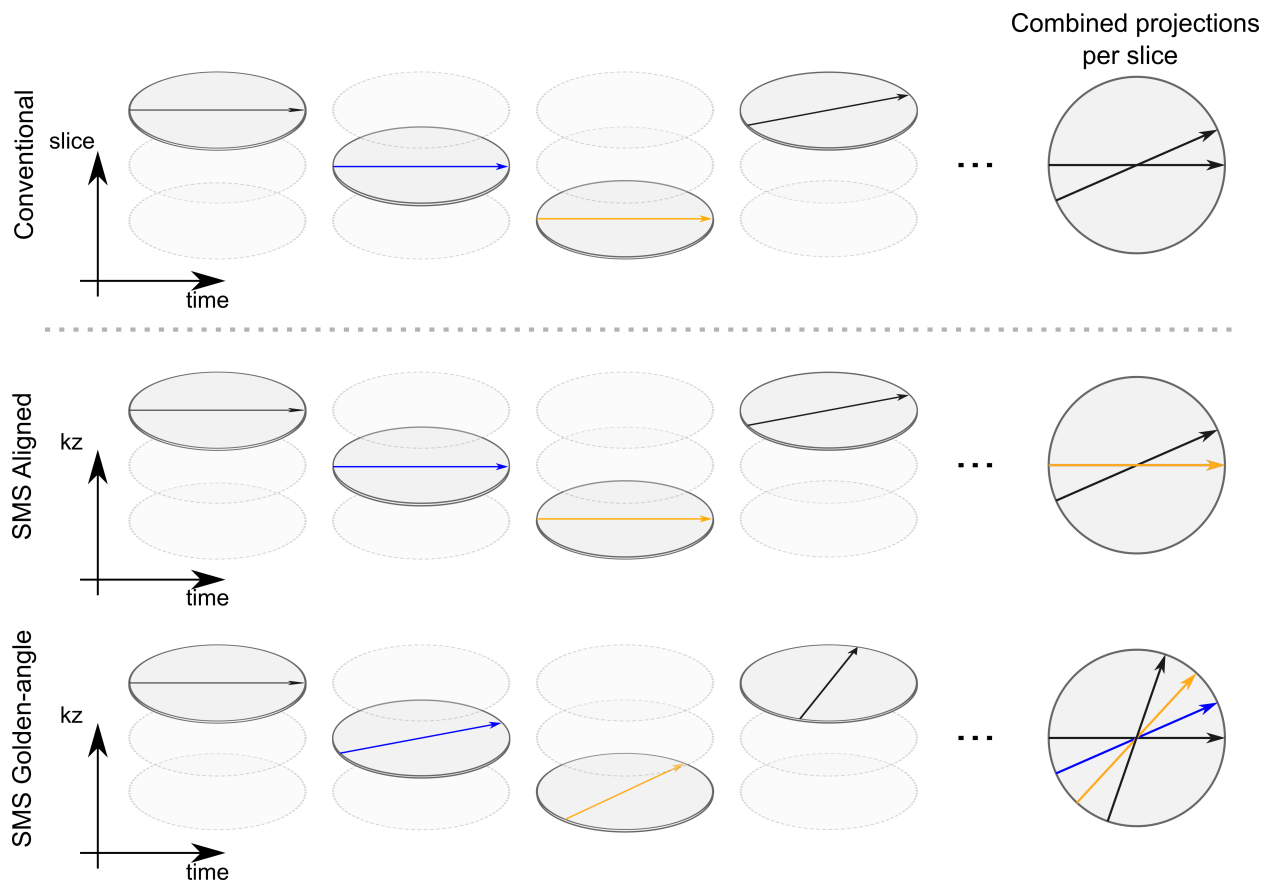


Figure 6: **Additional Figure 1.** IR radial multi-slice data acquisition schemes. (Top left) Conventional multi-slice acquisition scheme. (Middle and bottom left) Radial SMS with spokes distributed with aligned angles and rotated golden angles in the partition dimension, respectively. Note the longitudinal axis represents slice dimension for the conventional multi-slice scheme while partition dimension for the SMS acquisitions. (Right) Combined spokes for the first slice within the first 4 TRs for all schemes.

## Additional Files

Table 1: **Additional Table 1.** T1 relaxation times (ms, mean  $\pm$  SD) for the experimental phantom in Figure 1.

Tube	IR Spin-echo	Single-slice	SMS Golden-angle		
			Slice 1	Slice 2	Slice 3
1	315 $\pm$ 6	317 $\pm$ 4	335 $\pm$ 7	332 $\pm$ 7	324 $\pm$ 7
2	497 $\pm$ 8	460 $\pm$ 6	477 $\pm$ 11	473 $\pm$ 10	472 $\pm$ 12
3	661 $\pm$ 8	632 $\pm$ 8	654 $\pm$ 8	649 $\pm$ 7	648 $\pm$ 11
4	822 $\pm$ 12	800 $\pm$ 8	814 $\pm$ 11	806 $\pm$ 12	805 $\pm$ 14
5	1191 $\pm$ 13	1164 $\pm$ 18	1184 $\pm$ 15	1179 $\pm$ 21	1172 $\pm$ 19
6	1508 $\pm$ 15	1482 $\pm$ 21	1498 $\pm$ 23	1495 $\pm$ 24	1487 $\pm$ 24